

Evaluation of the DATTUTDUT model for predicting evapotranspiration in cowpea plants using thermal imaging¹

Avaliação do modelo DATTUTDUT na predição da evapotranspiração do feijão-caupi com imagens térmicas

Aderson S. de Andrade Júnior^{2*}, Amanda H. S. Sobral³, Edson A. Bastos²,
Raphael A. das C. N. Casari⁴, Henrique L. Roig⁴ & Magna S. B. de Moura⁵

¹ Research developed at Embrapa Meio-Norte, Teresina, PI, Brazil

² Embrapa Meio-Norte, Teresina, PI, Brazil

³ Universidade Federal do Piauí/Programa de Pós-graduação em Agronomia, Teresina, PI, Brazil

⁴ Universidade de Brasília/Programa de Pós-graduação em Geociências Aplicada e Geodinâmicas/Laboratório de Geoprocessamento, Brasília, DF, Brazil

⁵ Embrapa Agroindústria Tropical, Fortaleza, CE, Brazil

HIGHLIGHTS:

The DATTUTDUT model accurately estimates evapotranspiration in cowpea plants.

QGIS QWaterModel plugin performs well in estimating evapotranspiration with the DATTUTDUT model.

Local measurements of global and net solar radiation and air temperature improve the performance of the DATTUTDUT model.

ABSTRACT: Models based on surface temperature have been promising for predicting evapotranspiration. This study aimed to evaluate the DATTUTDUT model in predicting the evapotranspiration of cowpea BRS-Inhuma using images from a portable thermal camera. The research was conducted between September and October 2022 at the Embrapa Meio-Norte experimental station in Teresina, Piauí state, Brazil. Cowpea evapotranspiration was measured on hourly and daily scales using three weighing lysimeters. Thermal images were acquired 19, 26, 29, 37, 43, and 57 days after sowing. The model performance was evaluated by comparing the evapotranspiration values obtained from the images with those measured by weighing lysimeters on hourly and daily scales. Pearson's correlation coefficient (r), mean absolute error (MAE), and root mean square error (RMSE) were used to evaluate the model. The DATTUTDUT model based on surface temperature is promising for predicting cowpea evapotranspiration, with satisfactory performance on an hourly scale ($r = 0.9915$, $p \leq 0.001$; MAE = 0.015 mm per hour; and RMSE = 0.018 mm per hour) and a daily scale ($r = 0.9867$, $p \leq 0.001$; MAE = 0.21 mm per day; and RMSE = 0.242 mm per day).

Key words: *Vigna unguiculata* L. Walp, precision agriculture, QGIS, QWater plugin

RESUMO: Modelos baseados em temperatura de superfície têm sido promissores para predição da evapotranspiração. O objetivo do estudo foi avaliar o modelo DATTUTDUT para predição da evapotranspiração do feijão-caupi cv. BRS-Inhuma usando imagens de uma câmera térmica portátil. A pesquisa foi conduzida, entre setembro e outubro de 2022, na estação experimental da Embrapa Meio-Norte, no município de Teresina, Estado do Piauí, Brasil. A evapotranspiração do feijão-caupi foi medida em escalas horária e diária usando três lisímetros de pesagem. As imagens térmicas foram adquiridas aos 19, 26, 29, 37, 43 e 57 dias após a semeadura. O desempenho do modelo foi avaliado comparando os valores de evapotranspiração obtidos nas imagens com aqueles medidos por lisímetros de pesagem em escalas horária e diária. O coeficiente de correlação de Pearson (r), o erro absoluto médio (MAE) e a raiz do erro quadrático médio (RMSE) foram usados para avaliação do modelo. O modelo DATTUTDUT baseado na temperatura da superfície é promissor para predição da evapotranspiração do feijão-caupi, com desempenho satisfatório em escala horária ($r = 0,9915$, $p \leq 0,001$; MAE = 0,015 mm por hora; e RMSE = 0,018 mm por hora) e em escala diária ($r = 0,9867$, $p \leq 0,001$; MAE = 0,21 mm por dia; e RMSE = 0,242 mm por dia).

Palavras-chave: *Vigna unguiculata* L. Walp, agricultura de precisão, QGIS, QWater plugin

• Ref. 289380 – Received 14 Aug, 2024

* Corresponding author - E-mail: aderson.andrade@embrapa.br

• Accepted 07 Mar, 2025 • Published 31 Mar, 2025

Editors: Antônio Gustavo de Luna Souto & Carlos Alberto Vieira de Azevedo

This is an open-access article distributed under the Creative Commons Attribution 4.0 International License.



INTRODUCTION

Cowpea (*Vigna unguiculata* L. Walp) is an important crop and the main source of plant protein for the population in the Northeast region of Brazil (Silva et al., 2024). In the 2022/2023 crop season, 1,035,900 ha were cultivated with cowpea in the Northeast region, producing 441,200 tons and an average grain yield of 426 kg ha⁻¹ (CONAB, 2023). Cowpea is essentially grown under rainfed conditions, which has resulted in significant production losses in years with low rainfall depth. However, this crop has a high yield potential when grown under irrigation, as it is grown in important production areas in the Northeast and Central-West regions of Brazil (Castro Junior et al., 2015).

Increases in the grain yield potential of cowpea plants under irrigation conditions depend on the use of practices that improve water use efficiency, such as rational irrigation management with adequate water application during the crop season, which requires quantification of crop evapotranspiration (ETc) at the different crop development stages. The methods used for quantifying ETc include soil water balance (Allen et al., 1998) and weighing lysimeters (Campeche et al., 2011). However, these methods are expensive, labor-intensive, and require the installation of field devices, such as soil moisture sensors, weighing systems coupled with electronic load cells, and dataloggers; thus, they are recommended for use in experimental research areas (Campeche et al., 2011).

Studies estimating ETc through models with remote sensing techniques have focused on evaluating water use efficiency in agriculture, mainly in regions with water scarcity (Silva et al., 2019). Mapping temporal and spatial ETc enables the identification of variations in the field, which is useful for evaluating soil moisture conditions and crop water status (Vale et al., 2022).

Technical literature on this subject has presented several models that can be used for estimating ETc; the most used are SEBAL (Surface Energy Balance Algorithm for Land) and METRIC (Mapping Evapotranspiration at High Resolution with Internalized Calibration); however, these models are more complex (Silva et al., 2019). Simpler and less complex models that accurately predict ETc include SAFER - Simple Algorithm for Evapotranspiration Retrieving (Teixeira, 2010), DATTUTDUT -Deriving Atmosphere Turbulent Transport Useful to Dummies Using Temperature (Timmermans et al., 2015), and SSEBop - Simplified Operational Surface Energy Balance (Senay et al., 2022), which require data on canopy surface temperature for estimating ETc (Paula et al., 2019).

For many energy balance models, remotely sensed canopy surface temperatures are used as principal input, assuming that hot pixels result from low ETc and cold pixels indicate high ETc (Timmermans et al., 2015). A large variety of portable thermal cameras that can be attached to drones or used as handheld devices foster the use of energy balance modeling for ETc estimation (Xia et al., 2016), especially using plugins such as QWaterModel (Ellsäßer et al., 2020) to assist in image processing, without the need for much additional data.

Some studies have focused on evaluating ETc prediction models in crops, such as soybean - *Glycine max*, common bean

- *Phaseolus vulgaris*, wheat - *Triticum Aestivum*, grapevine - *Vitis vinifera*, and tropical palm - *Elaeis guineensis* (Xia et al., 2016; Paula et al., 2019; Ellsäßer et al., 2020; Vale et al., 2022), using the algorithms SSEBop, DATTUTDUT, and SAFER combined with orbital aerial images from Sentinel-2 and Landsat 8 satellites, as well as proximal images obtained by ARP. The results of these studies are promising for using models for estimating ETc in the evaluated crops.

Thermal images of crop canopy surfaces are an effective method for estimating ETc. In the case of cowpea, no study has yet focused on evaluating ETc prediction models using only thermal images of the crop canopy surface. In this context, the objective of the present study was to evaluate the DATTUTDUT model for predicting ETc in cowpea plants, comparing thermal images with data measured in weighing lysimeters.

MATERIAL AND METHODS

The study was conducted at the experimental station of the Brazilian Agricultural Research Corporation (Embrapa Mid-North) in the municipality of Teresina, Piauí state, Brazil (5° 05' S, 42° 29' W, and 72 m of altitude at sea level). Multispectral and thermal images were obtained from an area of 0.6 ha, where three weighing lysimeters were installed to quantify cowpea plants' evapotranspiration (ETc) (Figure 1).

The experimental area had a fixed conventional sprinkler irrigation system composed of eight lateral rows with sprinklers spaced at 12 m × 12 m intervals. The climate of the region, according to Köppen, was classified as Aw-type, with a wet summer (January - April) and a dry winter (May - November) (Medeiros et al., 2020). Historically, the area has presented annual average, maximum, and minimum temperatures of 28.2, 34, and 22.4 °C, respectively, annual average relative air humidity of 69.5%, and annual rainfall of 1,318 mm (Lopes et al., 2024).

Daily data on air temperature, relative air humidity, wind speed, global solar radiation, precipitation, and irrigation recorded during the study are presented in Figure 2. The average air temperature (Figure 2A) ranged from 29.2 to 29.9 °C, within the ideal range for cowpea development. The maximum air temperature reached 38.4 °C, the hottest day recorded 40 days after sowing (DAS). The optimum air temperature for cowpea development should be between 18 and 34 °C (Silva et al., 2024). Relative air humidity had a maximum of 90.5% at 25 days after sowing (DAS), and the lowest record was around 10% at 42 DAS (Figure 2B). The average wind speed was between 0.94 m s⁻¹ in the initial stage and 1.12 m s⁻¹ in the reproductive stage (Figure 2C). The average global solar radiation was 16.5 MJ m⁻² in the maturation stage and 19.3 MJ m⁻² in the initial stage (Figure 2D).

Irrigation management was based on fully meeting the reference evapotranspiration (ETo) demand, which was estimated daily using the Penman-Monteith method (Allen et al., 1998) with daily climate data obtained from an automatic weather station installed at 500 m from the experimental area. The total irrigation water depth applied to the experimental area from the sowing (August 31, 2022) to harvest (November

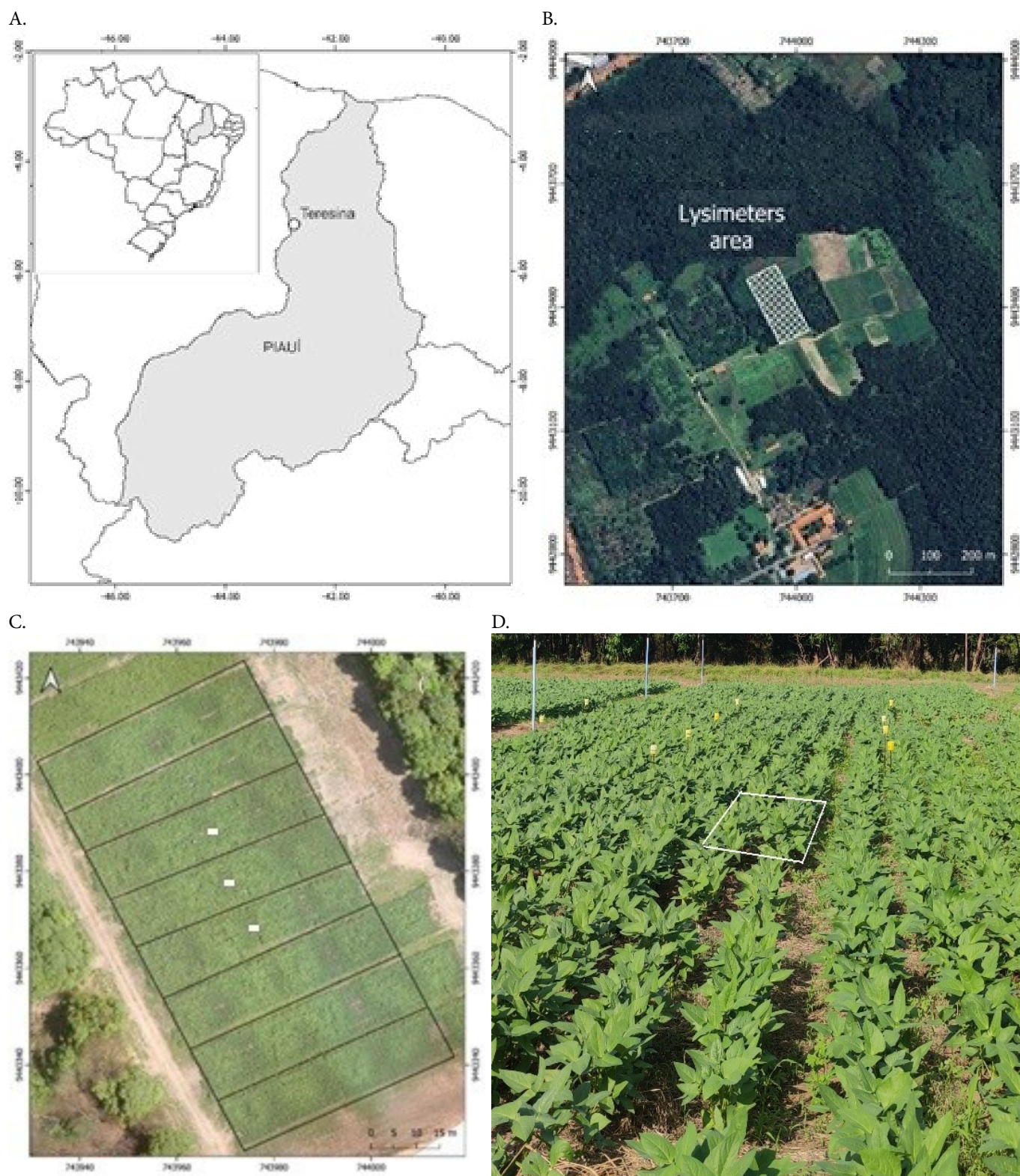


Figure 1. Location of Teresina city, Piauí state, Brazil (A), aerial image of the area with lysimeters (hatched area) (B), aerial image of the experimental area (border area-black lines and lysimeters-white rectangles) (C), and detail of one of the lysimeters-white rectangle (D)

01, 2022) was 194.7 mm over a total cycle of 63 days, with an average uniformity distribution of 74.5%. The total rainfall depth was 33.6 mm, resulting in a total water depth of 228.3 mm (irrigation plus rainfall) (Figure 2E).

The soil of the experimental area was classified as Argissolo Vermelho-Amarelo distrófico (Melo et al., 2019) or Ultisols (Soil Survey Staff (2022), whose chemical, physical, and hydrological characteristics are shown in Table 1, according

to the methodology proposed by Teixeira et al. (2017). Soil fertilizers were applied according to the soil analysis and recommendations for cowpea crops: 40 kg of P_2O_5 ha⁻¹ (triple superphosphate) and 40 kg of K_2O ha⁻¹ (potassium chloride) (Melo et al., 2020).

The cowpea evaluated was the BRS-Inhuma cultivar, which has an indeterminate growth habit, semi-prostrate plant, medium-early maturation cycle (70-75 days), pods inserted

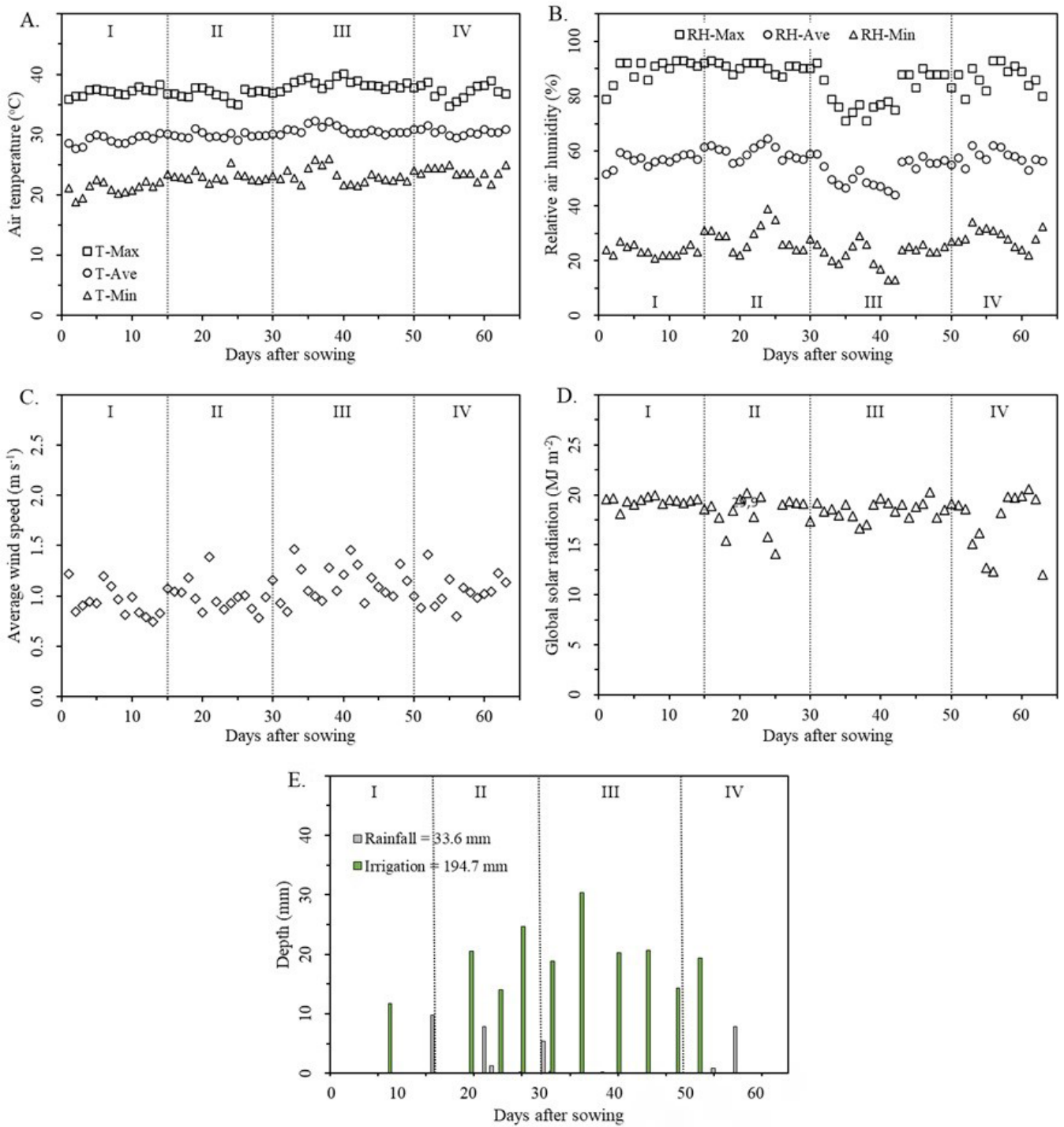


Figure 2. Air temperature (A), relative air humidity (B), average wind speed (C), global solar radiation (D), and rainfall and irrigation (E) during the cowpea growing season, cv. BRS Inhuma. Teresina, Piauí state, Brazil, 2022. Phases: I - Initial, II - Vegetative development, III - Reproductive, and IV - Maturation

Table 1. Chemical (fertility) and physical characteristics of the soil in the experimental area

Layer (m)	¹ OM	pH H ₂ O	² P (mg dm ⁻³)	² K ⁺	³ Mg ²⁺	³ Ca ²⁺	Al ³⁺	⁴ H+Al ³⁺	⁵ SB	⁶ CEC	⁷ V (%)
	(g kg ⁻¹)			(cmol _c dm ⁻³)	(cmol _c dm ⁻³)	(cmol _c dm ⁻³)					
0.0-0.2	12.9	5.8	31.12	0.09	0.35	0.78	0.11	1.86	1.13	2.94	42.32
0.2-0.4	11.2	6.0	23.49	0.09	0.42	0.73	0.22	2.04	1.15	2.89	44.11
Layer (m)	⁸ BD (g cm ⁻³)	Sand	Silt	Clay	Textural classification	⁹ θ _{cc}	¹⁰ θ _{pmf}				
								(g kg ⁻¹)	(g kg ⁻¹)	(%, volume)	
0.0-0.2	1.63	814.7	94.6	90.7	Sandy loam	21.9	5.8				
0.2-0.4	1.64	761.9	109.7	128.4	Sandy loam	20.8	6.3				

¹Organic matter, determined by colorimetry; ²Extractant: Mehlich-1; ³Extractant: 1M KCl; ⁴Extractant: 0.5 mol L⁻¹ Calcium acetate - pH 7.0; ⁵SB - Sum of bases; ⁶CEC - Cation exchange capacity; ⁷V - Base saturation; ⁸Bulk density; ⁹Field capacity and ¹⁰Permanent wilting point

above the foliage, and medium-sized grains, rhomboid shape, and brown color. Sowing was conducted on August 31, 2022, using a seeder-fertilizer with four rows spaced 0.5 m apart, set to sow ten seeds per meter (15 plants m⁻²). The harvesting of the dry pods and subsequent threshing of the dry grains were conducted manually on November 1, 2022.

Crop evapotranspiration (ET_c) was quantified on hourly and daily scales using three weighing lysimeters installed in the center of a 1.2 ha area, where 0.6 ha were grown with cowpea. The border area was occupied by other irrigated crops to remove the advection effect on the area with lysimeters (Figure 1C). Each lysimeter had a fiberglass container with a surface area of 2.25 m² (1.5 × 1.5 m) and a depth of 1 m. The lysimeters were supported by a lever mechanism connected to an electronic load cell and an automatic data collection and storage system (Datalogger).

Leaf area was quantified during the cowpea cycle at 19, 26, 33, 40, 47, and 54 days after sowing, using a ceptometer (Accupar, LP-80; Decagon Devices, Pullman, USA), which measures the leaf area index by calculating the ratio between the mean active photosynthetically radiations above and below the plant canopy. Measurements were taken in plants within the weighing lysimeter area and in the border area, with five replications. The LAI measurements were compared using the Tukey test at 5% probability. The RBIO software (Bhering, 2017) was used for this analysis.

Thermal images were captured using a thermographic module (Flir One Pro; Flir Systems, Portland, USA) with the following characteristics: thermal resolution of 160 × 120 pixels, RGB resolution of 640 × 480 pixels, temperature range of -20 to 120 °C, thermal sensor with a pixel of 12 μm, and a spectral range of 8 to 14 μm (www.flir.com.br/products/flir-one-pro). The thermographic module was coupled with a smartphone (iOS operational system). Images were captured at a height of 1.5 m, focusing on weighing lysimeters and the border areas at 19 (September 19, 2022), 23 (September 23, 2022), 29 (September 29, 2022), 37 (October 07, 2022), 43 (October 13, 2022), and 57 (October 27, 2022) days after sowing, between 10:00 a.m., and 12:00 p.m. The images were captured using automatic calibration mode for the following parameters: emissivity (0.95), reflected temperature (22.0 °C), atmospheric temperature (20.0 °C), external optics temperature (25.0 °C), external optics transmittance (1.0), and relative air humidity (50.0 %).

The thermal images were processed using the software Flir Tools (www.flir.com.br/products/flir-tools-app), involving the following phases: i) creation of a region of interest (ROI) containing only pixels within the lysimeter area (Figures 3A and B); ii) export of thermal images from the ROI to a .csv file; iii) obtaining of the highest temperature of the image, corresponding to the hot pixels, and calculation of the mean of the 0.5% lowest temperatures of the image, corresponding to cold pixels; and iv) development of histogram graphs of temperature of the pixel images in the ROI. Hot and cold pixels were determined to evaluate the DATTUTDUT model.

This energy balance model was introduced by Timmermans et al. (2015) and provides quick estimates of surface energy flux. It is a simple algorithm, requiring only a surface temperature image as input. The model is satisfactory for estimating energy

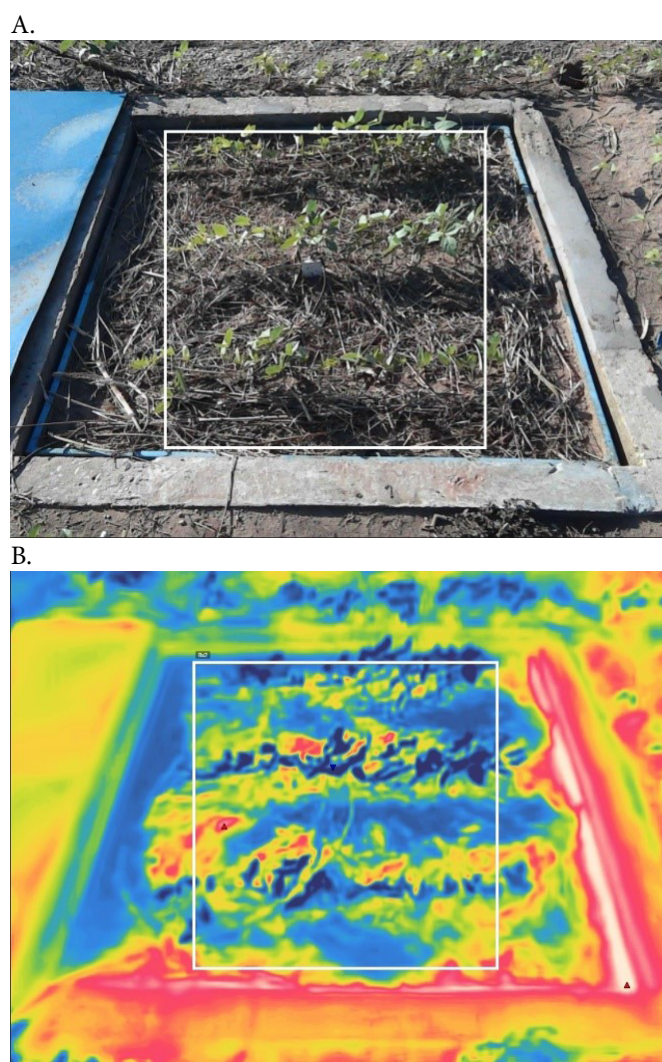


Figure 3. RGB (A) and thermal images (B) highlighting the region of interest (ROI) (40,000 pixels)

flux; however, there are some limitations for dry and partial canopy cover (Timmermans et al., 2015).

Surface radiometric temperature is an essential parameter of the surface energy state to determine key parameters for predicting the flux between the extremes of a cold/wet pixel under ET_c conditions at potential rate and hot/dry pixels essentially with no ET_c (Xia et al., 2016). The net solar radiation (R_n) is estimated from the balance between shortwave radiation and longwave radiation (Eq. 1) (Timmermans et al., 2015).

$$R_n = (1 - \alpha)R_s + \varepsilon_0 \varepsilon_a \sigma T_a^4 - \varepsilon \sigma T_0^4 \quad (1)$$

where:

- α - albedo (dimensionless);
- ε - effective emissivity (integrated soil + canopy emissivity) (dimensionless);
- σ - the Stefan-Boltzmann constant (5.6697 × 10⁻⁸ W m⁻² K⁻⁴);
- ε₀ - surface emissivity (dimensionless);
- ε_a - atmosphere emissivity (dimensionless);
- T - air temperature (K), with subscripts 0 and a representing the surface and atmospheric levels, respectively; and,
- R_s - calculated based on Sun-Earth astronomical relationships under cloudless sky conditions (Timmermans et al., 2015).

Nominal values of 0.7 and 0.96 for ϵ_a and ϵ , respectively, are assumed for model simplification (Xia et al., 2016).

The surface albedo varies linearly with the radiometric surface temperature between 0.05 and 0.25 (Eq. 2) (Timmermans et al., 2015):

$$\alpha = 0.05 + \left(\frac{T_0 - T_{\min}}{T_{\max} - T_{\min}} \right) 0.2 \tag{2}$$

where:

- Tmax (K) - is the maximum temperature;
- T₀ (K) - is the image temperature, and,
- Tmin (K) - is the 0.5% lowest temperature in the image.

The soil heat flux (G) is calculated based on the Rn with the coefficient Γ scaled between a minimum of 0.05 (full vegetation cover) and a maximum of 0.45 (bare soil). Thus, a linear relation with the radiometric surface temperature is assumed (Eq. 3) (Timmermans et al., 2015):

$$\Gamma = \frac{G}{R_n} = 0.05 + \left(\frac{T_0 - T_{\min}}{T_{\max} - T_{\min}} \right) 0.4 \tag{3}$$

A simple linear relation between Λ (evaporative fraction) and the extremes of surface temperature is assumed to Λ (Eq. 4) (Timmermans et al., 2015):

$$\Lambda = \frac{\lambda E}{\lambda E + H} = \frac{\lambda E}{R_n - G} = \left(\frac{T_{\max} - T_0}{T_{\max} - T_{\min}} \right) \tag{4}$$

This allows for the estimation of ETc on an hourly scale. The DATTUTDUT model adopts a simplified approach for estimating daily flux, assuming a constant evaporative fraction over the day. After estimating the evaporative fraction and assuming that soil heat flux is zero on a daily scale, the daily net radiation is estimated to obtain the daily latent heat, $\lambda_{E_{24}}$, both in MJ m⁻² (Eq. 5) (Timmermans et al., 2015):

$$\Lambda_i = \Lambda_{24} = \frac{\lambda E_i}{\lambda E_i + H_i} = \frac{\lambda E_{24}}{\lambda E_{24} + H_{24}} = \frac{\lambda E_{24}}{R_{n,24} - G_{24}} = \frac{\lambda E_{24}}{R_{n,24}} \tag{5}$$

Correcting the vaporization latent heat (MJ kg⁻¹) is needed for estimating daily rates of evaporated water and transpiration, E₂₄ (kg m⁻²). The vaporization latent heat (λ) is dependent on air temperature, considering the Tmin (K) (Eq. 6) (Timmermans et al., 2015):

$$\lambda = 2.501 - 0.002361(T_{\min} - 273.15) \tag{6}$$

The QGIS QWaterModel plugin was used for estimating ETc with the DATTUTDUT model (Ellsäßer et al., 2020), whose input parameters are shown in Table 2. Local measurements of essential parameters that optimize ETc estimates, such as global and net solar radiation and air temperature during thermal image acquisition (UTC hour), were input into the plugin to run the DATTUTDUT model. Hourly Rs were obtained from online data from an automatic Brazilian National Institute of Meteorology (INMET) station installed 500 m from the area with lysimeters. Rn was estimated based on Rs, and coefficients were determined for local conditions by Andrade Junior et al. (2017). Tmin and Tmax of the surface thermal images of lysimeters were obtained as previously described.

Standard values of G, ϵ_0 , ϵ_a , and τ recommended by Ellsäßer et al. (2020) were used. Although optional parameters, coordinates (latitude and longitude) and altitude of the center of the area with lysimeters were inserted into the model. Energy flux balance (sensible and latent heat of evaporation) and ETc were estimated on an hourly scale (3600 s) (Table 2).

ETc, in mm, was estimated on hourly and daily scales using the ET0, according to the Penman-Monteith model (Allen et al., 1998), with climate data from an automatic station of INMET installed at 500 m from the area with lysimeters.

The QWaterModel plugin exports DATTUTDUT model results in raster images containing bands for net radiation (Rn, W m⁻²), latent heat flux (W m⁻²), sensible heat flux (W m⁻²), soil heat flux (W m⁻²), evaporative fraction (Λ , %), and evapotranspiration (ETc, mm h⁻¹) in .csv files (sheets) containing the input data and average, maximum, and

Table 2. Input parameters of the DATTUTDUT model in the QGIS QWaterModel plugin

Parameters		09/19/22	09/23/22	09/29/22	10/07/22	10/13/22	10/27/22
Hour (UTC)		13:20:40	13:44:34	14:34:32	13:09:56	14:28:10	14:41:03
Tmin (K)	Lys-1	305.4	302.0	301.0	299.4	301.4	305.1
	Lys-2	303.9	300.9	300.3	299.5	301.3	305.7
	Lys-3	309.4	296.1	301.3	300.0	301.2	306.0
Tmax (K)	Lys-1	320.0	313.1	311.9	305.2	306.7	320.5
	Lys-2	318.6	313.3	314.5	309.8	308.1	316.5
	Lys-3	319.5	307.9	309.9	305.4	309.0	320.3
Rs (W m ⁻²)		479.6	649.3	620.3	675.3	690.2	650.4
Rn (W m ⁻²)		335.7	454.5	434.2	472.7	483.1	455.3
G (%)		10	10	10	10	10	10
ϵ_0		1.0	1.0	1.0	1.0	1.0	1.0
ϵ_a		0.8	0.8	0.8	0.8	0.8	0.8
τ		0.7	0.7	0.7	0.7	0.7	0.7
Tar (K)		303.9	302.9	303.5	304.7	306.3	304.9
T (s)		3600	3600	3600	3600	3600	3600

Tmin - Minimum surface temperature (K); Tmax - Maximum surface temperature (K-Kelvin); Rs - Global solar radiation (W m⁻²); Rn - Net solar radiation (W m⁻²); G - Soil heat flux (%); ϵ_0 - Surface emissivity; ϵ_a - Atmospheric emissivity; τ - Atmospheric transmissivity; Tar - Air temperature (K); T - Time for energy flux estimation (s); coordinates of the location (Teresina, PI, Brazil. Long.: -42.8037597, Lat.: -5, 0920108, Alt.: 72 m). Lys - Lysimeter

minimum values of raster bands (Ellsäßer et al., 2020). Values were extracted from the thermal images, and histograms were developed with pixel distribution in classes of occurrence (%). The number of classes (NC) was defined by the Sturges' formula: $NC = 1 + [3.3 * \text{Log}(n)]$, where n is the number of evaluated pixels. Only pixels from the vector layer used as a 40,000-pixel ROI were considered (Figure 2), resulting in an NC of 16. E_{Tc} values obtained from the images were correlated with measurements from the weighing lysimeters on hourly and daily scales to assess the model's performance.

The Pearson correlation coefficient (r) (Eq. 7) was used to evaluate the performance of the E_{Tc} prediction models by the DATTUTDUT model, with significance level defined by the t-test, mean absolute error (MAE) (Eq. 8), and root mean square error (RMSE) (Eq. 9) (Xia et al., 2016; Ellsäßer et al., 2020).

$$r = 1 - \frac{\sqrt{\sum_{i=1}^n (y_i - \hat{y}_i)^2}}{\sqrt{\sum_{i=1}^n (y_i - \bar{y}_i)^2}} \quad (7)$$

$$MAE = \frac{1}{n} \sum_{i=1}^n |y_i - \hat{y}_i| \quad (8)$$

$$RMSE = \sqrt{\frac{\sum_{i=1}^n (y_i - \hat{y}_i)^2}{n}} \quad (9)$$

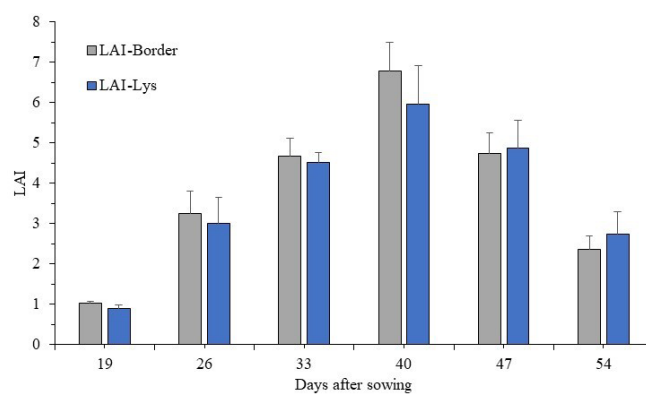
where:

- n - is the number of observations;
- y_i - is the E_{Tc} measured in the field (mm);
- \hat{y}_i - is the E_{Tc} estimated by the DATTUTDUT prediction model (mm); and,
- \bar{y}_i - is the mean E_{Tc} measured in the field (mm).

RESULTS AND DISCUSSION

The leaf area index (LAI), measured during the cowpea developmental stage, using a ceptometer, on plants in the lysimeters (LAI-Lys) and in the border area (LAI-Border) is shown in Figure 4. There was no significant difference ($p > 0.05$) between the LAI-Lys and LAI-Border measurements. However, a small difference in absolute values was found between LAI in the lysimeters and the border area. LAI in the border area was slightly higher than in the lysimeters (LAI-Lys) up to 40 days after sowing (DAS), probably due to the lower initial development of plants in the lysimeters. The LAI curve increased from 19 to 40 DAS, ranging from 0.9 ± 0.09 to 5.9 ± 0.97 in the lysimeters. The LAI decreased after 40 DAS, presenting 4.9 ± 0.71 (47 DAS) to 2.7 ± 0.55 (54 DAS) (Figure 3). The highest LAI results were found at 40 DAS when the crop canopy reached full development.

Souza et al. (2017) conducted a test under rainfed and irrigated conditions in Castanhal, Pará state, Brazil, using the cowpea cultivar BR3-Tracuateua, and found the highest



Error bars represent the standard deviation of the LAI measurements ($n=3$ for LAI-Lys, and $n=5$ for LAI-Border)

Figure 4. Leaf area index (LAI) of cowpea cv. BRS Inhuma measured on plants inside the lysimeters (LAI-Lys) and in the border area (LAI-Border) at different days after sowing (DAS)

LAI for the irrigated treatment: 3.29 ± 0.15 at 48 DAS in 2012 and 3.26 ± 0.19 at 50 DAS in 2013, during the reproductive stage. Under rainfed conditions, the highest LAI was 1.75 ± 0.09 (2012) and 2.84 ± 0.17 (2013), denoting decreases of approximately 46.8 and 12.9%, respectively, compared to the irrigated treatment. The results show that cowpea plants do not maintain leaf area production when subjected to water stress. The decreases in leaf area may be due to a survival strategy of the plants for reducing leaf surface transpiration (Bastos et al., 2011; Digrado et al., 2020). The LAI results found by Souza et al. (2017) were lower than those found in the present study, probably due to differences in the methodology used to determine LAI, the growth habit and cycle of the cultivars used, and the water and solar radiation availability during the experiments, which directly affected crop growth (Bastos et al., 2012; Digrado et al., 2022).

The variability of surface temperatures in the weighing lysimeters and border areas and their percentages of distribution in classes of occurrence in the central region of the lysimeters are shown in Figures 4 and 5. Surface temperature variability was evident during the cowpea developmental stage.

The highest surface temperatures were found at the initial and final cowpea developmental stages (Figure 5). During the initial stage (19 DAS), the mean surface temperature was 39.1 ± 2.1 °C, with a maximum of 46.0 °C and a minimum of 30.7 °C. During the final stage (57 DAS), the mean surface temperature was 38.0 ± 1.6 °C, with a maximum of 44.5 °C and a minimum of 33.1 °C. There was a high thermal amplitude during these stages, from 15.3 °C (19 DAS) to 11.4 °C (57 DAS). The spatial distribution of the surface temperature showed that 76.8% of surface temperatures ranged from 36.5 to 40.3 °C at 19 DAS, and 68% had temperatures from 36.6 to 38.7 °C at 57 DAS (Figures 5A and F). The higher predominance of soil pixels between plant rows, with higher temperatures, was responsible for these high surface temperatures, as the plants presented lower LAI due to the lower initial growth (19 DAS) or leaf senescence (57 DAS) (Figure 4). Higher drying of the soil surface occurs during these plant stages, with more intensity under lower soil surface cover, which decreases soil moisture and, consequently, increases the albedo and surface temperature (Lima et al., 2013).

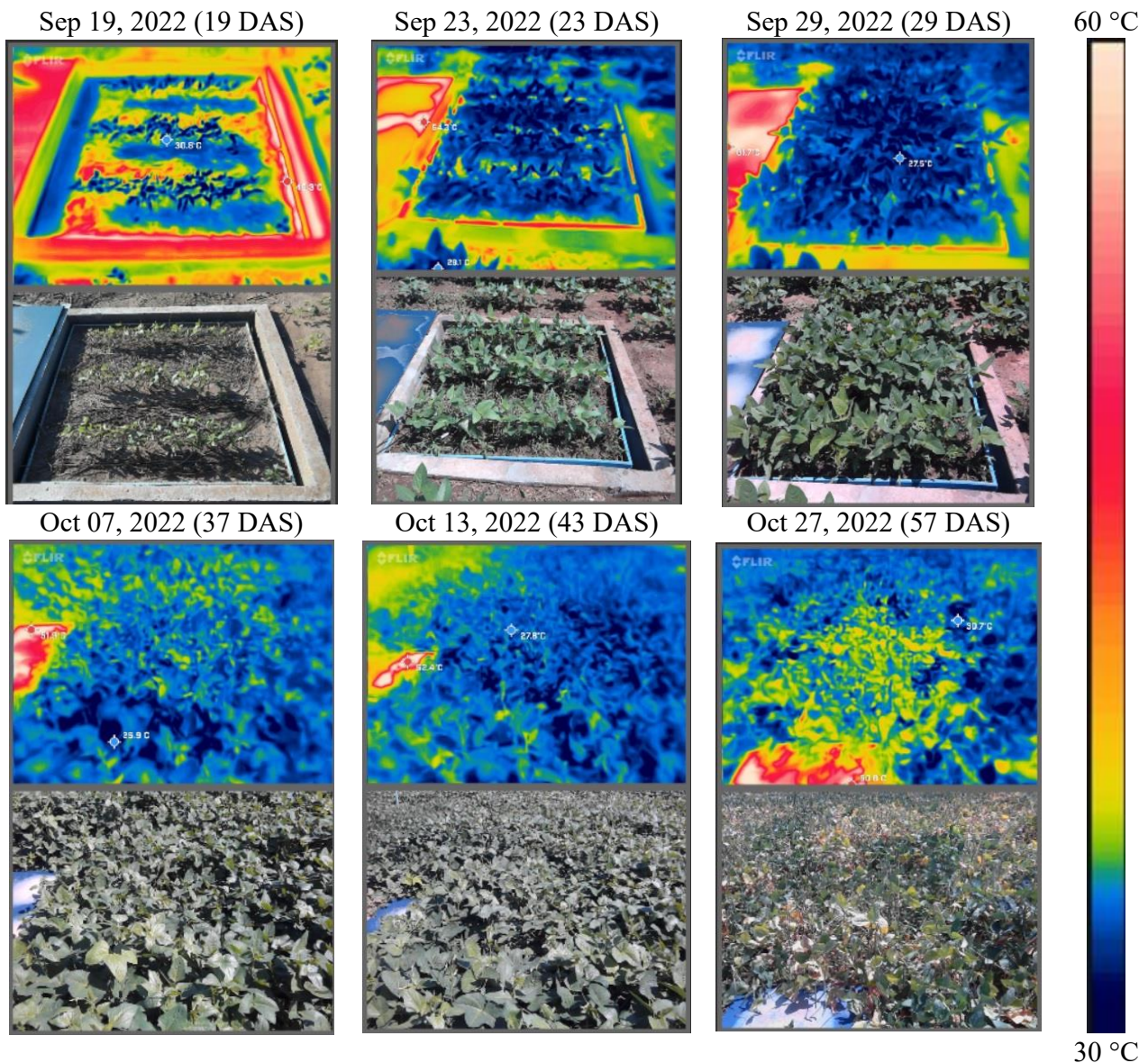


Figure 5. RGB (Red-Green-Blue) and thermal images of cowpea cv. BRS Inhuma in the area with weighing lysimeters and the border area

Surface thermal amplitude decreases during cowpea intermediate growth stages. The difference in temperature between hot and cold pixels was from 11.5 °C (23 DAS) to 5.1 °C (43 DAS) (Figures 5B and E). The maximum and minimum temperatures varied from 32.1 to 26.6 °C (Figure 5D) and 39.1 to 28.4 °C (Figure 5B). Increases in cowpea leaf area are more intense during these stages (30 to 45 DAS) (Figure 3), presenting higher LAI during full flowering stage and the beginning of pod formation (Ayalew et al., 2022), thus decreasing the occurrence of soil pixels with higher temperature.

The temperature variation between hot and cold pixels in the thermal images determines the intensity of energy fluxes (latent, sensible, and soil heat), which affect the ETC of crops (Timmermans et al., 2015; Xia et al., 2016). The maximum (hot pixels) and minimum (0.5% of cold pixels) temperatures found in the lysimeters (ROI = 40000 pixels) were presented in Table 2; they were used for predicting the ETC of cowpea by the DATTUTDUT model.

The output parameters of the DATTUTDUT model (Timmermans et al., 2015) using the QGIS QWaterModel

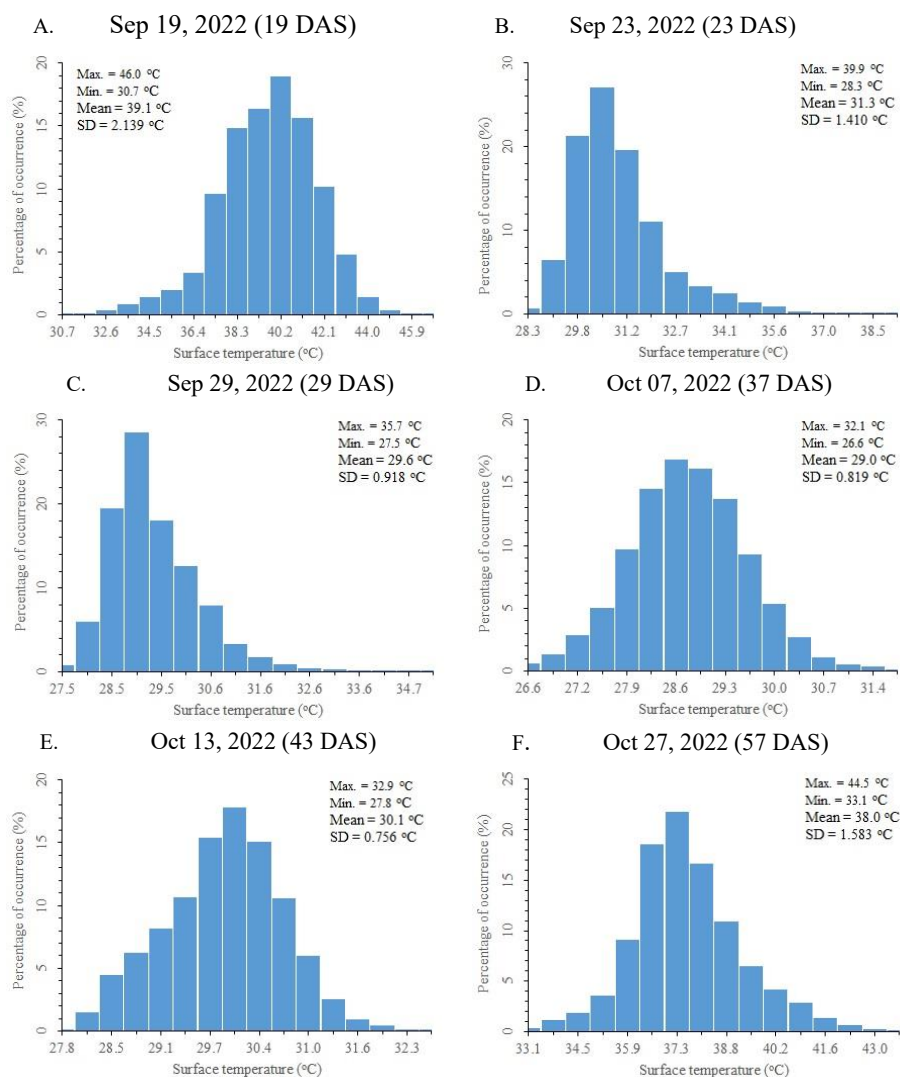
plugin (Ellsäßer et al., 2020) are shown in Table 3. The surface albedo decreased from 0.148 ± 0.016 (19 DAS) to 0.058 ± 0.011 (29 DAS) and then increased to 0.126 ± 0.020 (43 DAS) and 0.118 ± 0.035 (57 DAS). Albedo is the quantity of solar radiation reflected by a surface concerning solar radiation (Allen et al., 1998); it is related to temperature and latent and sensible surface heat fluxes (Lima et al., 2013). Higher surface temperatures (hot pixels) predominated during the initial (19 DAS and 23 DAS) and final (43 and 57 DAS) developmental crop stages due to uncovered soil and/or leaf senescence, whereas lower surface temperatures (cold pixels) predominated during intermediate stages (29 and 37 DAS) due to higher increases in leaf area (Figure 6).

The results found for LE and H fluxes were consistent with the variability in albedo and surface temperature during the cowpea cycle (Figure 6). LE presented increases, following increases in cowpea leaf area, between 19 DAS (LE = $146.5 \pm 28.0 \text{ W m}^{-2}$) and 29 DAS (LE = $347.0 \pm 33.5 \text{ W m}^{-2}$) (Figure 3), stabilization during intermediate stages, at 37 DAS (LE = $337.9 \pm 58.9 \text{ W m}^{-2}$) and 43 DAS (LE = $315.8 \pm 68.4 \text{ W m}^{-2}$),

Table 3. Means and standard deviations of the output parameters of the DATTUTDUT model using the QGIS QWaterModel plugin and the respective fractions between the components of the energy balance at different days after sowing (DAS)

Parameters	09/19/2022 (19 DAS)	09/23/2022 (23 DAS)	09/29/2022 (29 DAS)	10/07/2022 (37 DAS)	10/13/2022 (43 DAS)	10/27/2022 (57 DAS)
α_0	0.148 ± 0.016	0.094 ± 0.035	0.058 ± 0.011	0.064 ± 0.005	0.126 ± 0.020	0.118 ± 0.035
LE (W m ⁻²)	146.5 ± 28.0	247.2 ± 58.1	347.0 ± 33.5	337.9 ± 58.9	315.8 ± 68.4	295.3 ± 37.9
H (W m ⁻²)	188.8 ± 28.0	206.9 ± 58.1	86.7 ± 33.5	134.3 ± 58.9	167.2 ± 68.4	164.0 ± 37.9
G (W m ⁻²)	0.45	0.45	0.45	0.45	0.45	0.45
Λ	0.437 ± 0.08	0.544 ± 0.13	0.800 ± 0.08	0.716 ± 0.11	0.650 ± 0.16	0.640 ± 0.08
ETc (mm h ⁻¹)	0.217 ± 0.04	0.366 ± 0.08	0.514 ± 0.05	0.501 ± 0.08	0.459 ± 0.12	0.432 ± 0.06
Rn (W m ⁻²)	335.7	454.5	434.2	472.7	483.1	455.3
LE/Rn	0.437	0.544	0.799	0.715	0.650	0.640
H/Rn	0.562	0.455	0.200	0.284	0.349	0.359

DAS - Days after sowing; α_0 - Surface albedo; LE - Latent heat flux; H - Sensible heat flux; G - Soil heat flux; Λ - Evaporative fraction; ETc - Hourly evapotranspiration; Rn - Net solar radiation LE/Rn - Ratio LE/Rn; H/Rn - Ratio H/Rn. Data obtained only from the area with lysimeters (ROI = 40,000 pixels)



DAS - Days after sowing; Max. - Maximum; Min. - Minimum; SD - Standard deviation

Figure 6. Histograms of surface temperature of cowpea plants in weighing lysimeter 2. Data from the lysimeter area only (ROI = 40,000 pixels)

and decreases during the final stage, at 57 DAS (LE = 295.3 ± 37.9 W m⁻²) due to the senescence of plants (Table 3).

However, H presented an opposite behavior compared to LE flux, with decreases during the initial stages, at 19 DAS (H = 188.8 ± 28.0 W m⁻²) to 29 DAS (H = 86.7 ± 33.5 W m⁻²) and increases during the following stages, at 37 DAS (H = 134.3 ± 58.9 W m⁻²), 43 DAS (H = 167.2 ± 68.4 W m⁻²), and 57 DAS (H = 164.0 ± 37.9 W m⁻²). The soil heat flux was considered in the model (Table 2); thus, it was assumed to remain constant

throughout the cowpea cycle, representing 10% of the balance (Rn) (Table 3).

Lima et al. (2013) found increased LE and decreased H measured by a micrometeorological tower installed at the center of the experimental area, with increases in cowpea leaf area, when conducting a test under rainfed conditions in Areia city, Paraíba state, Brazil. During the vegetative stage (27 DAS), with a soil cover fraction of ≈ 35%, Lima et al. (2013) found similar hourly LE and H, close to 200 W m⁻²; during

the reproductive stage (67 DAS), with a soil cover fraction of $\approx 95\%$, LE was the main component of energy balance, with a mean of 400 W m^{-2} , whereas H was 100 W m^{-2} . During the senescence stage (82 DAS), with a soil cover fraction of $\approx 80\%$, there were decreases in LE (300 W m^{-2}) and H (150 W m^{-2}). However, the cultivar used in the study presented a total cycle of 90 days, which is long compared to current cultivars of early maturation cycle (65 days). Nevertheless, LE and H results were similar to those found in the present study.

The lowest LE/Rn, which corresponds to the evaporative fraction (λ), was found during the vegetative stage, at 19 DAS (0.437) and 23 DAS (0.544) (Table 3), as lower soil cover is common during this stage (Figure 3), with available energy (Rn) being used for H, whose fractions varied from 0.562 (19 DAS) to 0.455 (23 DAS) (Table 3). During the reproductive stage, the LE/Rn fraction increased to 0.800 (29 DAS) and 0.716 (37 DAS), and H/Rn decreased to 0.200 (29 DAS) and 0.284 (37 DAS) (Table 3), as the maximum LAI was reached during this stage (Figure 3). During the grain formation and maturation stages (43 and 57 DAS), LAI decreases (Figure 3), whereas LE/Rn and H/Rn fractions were stable (LE/Rn ≈ 0.65 and H/Rn ≈ 0.35) (Table 3). The means during the cowpea cycle were LE/Rn = 0.633 and H/Rn = 0.368.

Lima et al. (2013) evaluated cowpea crops and found that the largest part of Rn was used as LE, with a mean of 0.73 ± 0.10 throughout the crop cycle. The lowest LE/Rn results (0.50-0.66) were found for the bare soil and between 16 and 19 DAS (0.54-0.58) when the soil water content was low. Lima et al. (2013) found that the lowest LE/Rn values (~ 0.55 -0.58) occurred after a sequence of days with no rain when the soil water was reduced, while the ratio LE/Rn rapidly increased after rains events with more than 20 mm. The opposite was observed by Lima et al. (2013) for the H/Rn relationship. The mean H/Rn was 0.18 ± 0.07 , with a maximum from 0.25 to 0.40 during the crop's initial developmental stage and between 16 and 20 DAS in the less rainy period. H/Rn was stable (0.18) from 40 to 79 DAS, probably due to the higher soil cover during these stages, with increases during the senescence stage due to the low soil cover. Lima et al. (2013) also verified the same behavior and similar average value (H/Rn = 0.18). These authors found that the mean G/Rn was 0.09 ± 0.04 , with a maximum from 0.14 to 0.18 at the initial stage, when the soil cover was still low, and in periods when the soil water content was low. The methodology approach here assumes a fixed ratio for G/Rn, as proposed by Ellsäßer et al. (2020). The results of the fluxes found by Lima et al. (2013) were similar to those found in the present study.

The observed relationship between energy fluxes and cowpea plants can be explained by analyzing how the crop interacts with energy at the Earth's surface, primarily through its response to net radiation (Rn) and its partitioning into latent heat flux (LE), sensible heat flux (H), and soil heat flux (G). This relation depends on the crop water status reflecting the soil moisture and gas exchange between the crop and atmosphere and the crop cover, as presented by LAI in Figure 4.

Net radiation is the primary driver of energy exchanges in cowpea fields. It represents the balance between incoming and outgoing solar and longwave radiation, influenced by the crop's albedo (reflectivity) and canopy characteristics. Higher

Rn typically coincides with favorable photosynthetic activity during the cowpea growing season, contributing to biomass accumulation. Rn is partitioned into LE, H, and G, and its ratio is driven by different factors that essentially alter the soil-plant-atmosphere relation, such as the crop species, irrigation system, soil water availability, plastic cover, till management (Allen et al., 1998; Lima et al., 2013).

Latent heat flux, associated with evapotranspiration (ET), is the dominant energy sink in well-watered cowpea systems. As cowpea has moderate water-use efficiency, LE increases with soil moisture availability, reflecting the water vapor released from the soil and transpired by the crop. This process regulates canopy temperature, promotes stomatal conductance, and is critical for maintaining physiological functions (Ferreira et al., 2021). On the other hand, sensible heat flux (H) often increases in water-limited conditions at the expense of LE due to reduced transpiration rates and can lead to higher canopy temperatures, potentially inducing thermal stress that limits photosynthetic efficiency and growth. Soil heat flux reflects energy stored or released in the soil. In cowpea fields, G is influenced by the crop's phenology, canopy coverage, and soil moisture. Early in the growing season, when canopy cover is minimal, G is higher due to increased solar radiation reaching the soil surface. As the canopy develops, G decreases, with more energy redirected toward LE (Allen et al., 1998; Lima et al., 2013).

The interplay between these fluxes varies throughout the cowpea growth cycle: for early growth stage, higher G and H, lower LE due to limited canopy cover; for mid-season, the maximum LE due to full canopy development and active transpiration; and for late growth stage happen a gradual reduction in LE as the crop senesces, with a corresponding increase in H.

Efficient water management is critical for optimizing LE, particularly in semi-arid environments where cowpea is commonly grown. Excessive H due to water deficits can exacerbate heat stress, reducing yield. Similarly, soil mulching, till management, or intercropping can modulate G, improving energy use efficiency in the soil-plant-atmosphere system.

Studies have indicated that flux variations in energy balance components (LE, H, and G) depend on soil coverage by crops and soil water availability by Lima et al. (2013). In the present study, variations in LE and H depended only on the cowpea leaf area index, as soil moisture was kept close to field capacity due to the irrigation management used. The fixed relationship for G/Rn was used, as proposed by Ellsäßer et al. (2020), once the daily G variation is small, considering daytime and nighttime energy input and output on the soil surface (Allen et al., 1998).

The ETc on the hourly scale varied from 0.217 ± 0.04 to $0.366 \pm 0.08 \text{ mm h}^{-1}$ during the vegetative stage (19 and 23 DAS), from 0.514 ± 0.05 to $0.501 \pm 0.08 \text{ mm h}^{-1}$ during the reproductive stage (29 and 37 DAS), and from 0.459 ± 0.12 to $0.432 \pm 0.06 \text{ mm h}^{-1}$ during the grain formation and maturation stage (Table 3). The variation in ETc depends on the evaporative fraction (λ) and ETo (Table 3). Thus, higher ETc were found during the reproductive stage, in which the highest evaporative fractions were found due to the higher leaf area available for the evapotranspiration process (Figure 4).

The analysis of the Pearson correlation coefficient (r) between the ET_c estimated by the DATTUTDUT model on hourly and daily scales and the ET_c measured in weighing lysimeters is shown in Figure 7.

The r values found were high on hourly (0.9915) and daily (0.9867) scales, with a high significance level by the t -test ($p \leq 0.001$). The indexes of model performance evaluation were $MAE = 0.015$ mm per hour and $RMSE = 0.018$ mm per hour on the hourly scale (Figure 7A), and $MAE = 0.21$ mm per day and $RMSE = 0.242$ mm per day on the daily scale (Figure 7B). Ellsäßer et al. (2020) evaluated the DATTUTDUT model for predicting ET_c in tropical palm plants, comparing images from a handheld thermal camera with ET_c measurements by a micrometeorological tower (Eddy Covariance method). They also found consistency between the measured and predicted ET_c data, with $r = 0.95$ ($p \leq 0.001$), $MAE = 0.05$ mm per hour, and $RMSE = 0.06$ mm per hour, similar to those found in the present study. They attributed this result to in-situ measurements of global radiation (R_g) and net radiation (R_n) used for predicting ET_c through the DATTUTDUT model, which significantly improved the overall accuracy of the model (Ellsäßer et al., 2020).

Additionally, handheld thermal cameras allow for the obtaining of images focused on the crop canopy, excluding

the presence of objects other than leaves in the images, which is common in images obtained using drones (Ellsäßer et al., 2020). The temperatures of objects that are not part of the crop canopy differ from the crop surface temperatures; these different temperatures strongly affect the ET_c prediction (Ellsäßer et al., 2020). This effect was also reported in a study that found significant differences in canopy temperature in grapevine crops (Xia et al., 2016). In the present study, in-situ measurements of R_g and R_n were used, and a region of interest in the area with lysimeters was defined for obtaining hot and cold pixels from thermal images focused only on cowpea canopy; together, these approaches favored a better ET_c prediction by the DATTUTDUT model. In practical terms, using a handheld thermal camera is viable for estimating ET_c in cowpea plants since the crop is grown in small areas.

CONCLUSIONS

1. The DATTUTDUT model, based on surface temperature, is promising for predicting evapotranspiration in cowpea cv. BRS Inhuma and presenting satisfactory performance on an hourly scale ($r = 0.9915$, $p \leq 0.001$; $MAE = 0.015$ mm per hour; and $RMSE = 0.018$ mm per hour) and on a daily scale ($r = 0.9867$, $p \leq 0.001$; $MAE = 0.21$ mm per day; and $RMSE = 0.242$ mm per day).

2. The use of thermal images of the canopy obtained by a handheld camera proved to be a promising, simple, and low-cost technique for quantifying ET_c in cowpea plants.

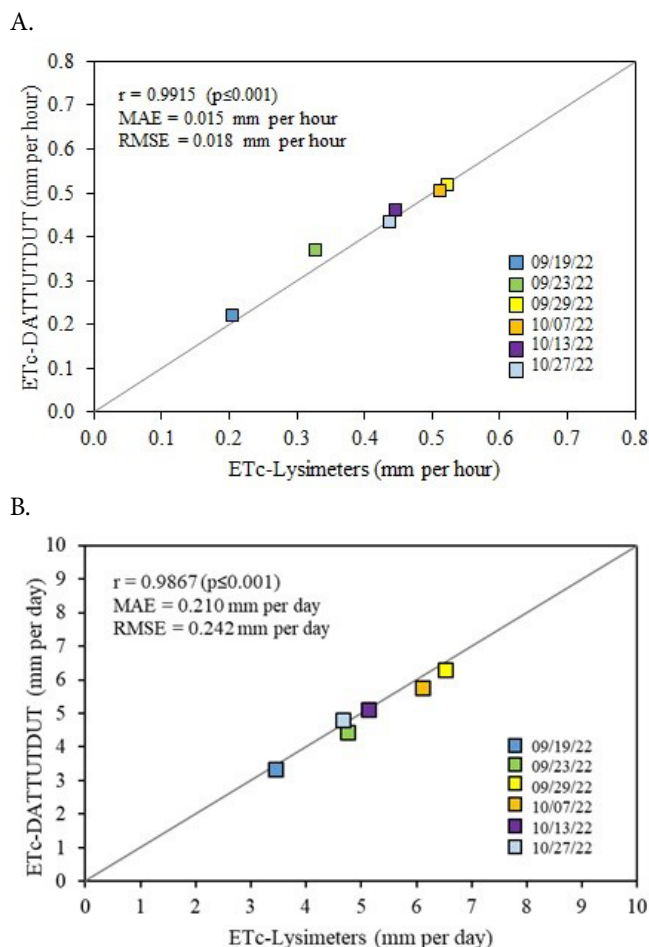
3. The QGIS plugin QWaterModel performs well in estimating evapotranspiration with the DATTUTDUT model. However, it is necessary to use local measurements of global and net solar radiation and air temperature to improve model performance.

4. Understanding the relationship between energy fluxes and cowpea growth is essential for predicting crop performance under varying environmental and management conditions, thereby informing sustainable agricultural practices. This study presents a simple method based on thermal imaging, using a free and public model (QWater), to help understand the relationship between energy fluxes and cowpea evapotranspiration.

Contribution of authors: Aderson Soares de Andrade Júnior: conceptualization, investigation, resource acquisition, methodology, data processing, software, statistical analysis, writing - original draft, writing - final draft. Amanda Hellen Sales Sobral: conceptualization, investigation, data processing, writing - original draft. Edson Alves Bastos: conceptualization, investigation, writing - original draft. Raphael Augusto das Chagas Noqueli Casari: conceptualization, data processing, writing - original draft. Henrique Roig: conceptualization, data processing, writing - original draft. Magna Soelma Beserra de Moura: conceptualization, data processing, software, writing - original draft, writing - final draft.

Supplementary documents: There are no supplementary sources.

Conflict of interest: The authors declare no conflict of interest.



r: Pearson correlation coefficient; p: significance level by the t -test; MAE: mean absolute error; RMSE: root mean square error. ET-DATTUTDUT means obtained only from the area with lysimeters (ROI = 40,000 pixels)

Figure 7. Correlation between cowpea evapotranspiration (ET_c) measured in lysimeters and estimated by the DATTUTDUT model on hourly (A) and daily scales (B)

Financing statement: The research was funded by the Brazilian Agricultural Research Corporation (EMBRAPA) - Financial Management System Code 20.22.01.011.00.06. 014

LITERATURE CITED

- Allen, R. G.; Pereira, L. S.; Raes, D.; Smith, M. Crop evapotranspiration: Guidelines for computing crop water requirements. Rome: FAO, 1998. 300p. Drainage and Irrigation Paper, 56
- Andrade Junior, A. S.; Noleto, D. H.; Bastos, E. A.; Moura, M. S. B.; Anjos, J. C. R. Demanda hídrica da cana-de-açúcar, por balanço de energia, na microrregião de Teresina, Piauí. *Agrometeoros*, v.25, p.229-238, 2017.
- Ayalew, T.; Yoseph, T.; Högy, P.; Cadisch, G. Leaf growth, gas exchange and assimilation performance of cowpea varieties in response to *Bradyrhizobium inoculation*. *Heliyon*, v.8, e08746, 2022. <https://doi.org/10.1016/j.heliyon.2022.e08746>
- Bastos, E. A.; Nascimento, S. P.; Silva, E. M.; Freire Filho, F. R.; Gomide, R. L. Identification of cowpea genotypes for drought tolerance. *Revista Ciência Agrônômica*, v.42, p.100-107, 2011. <https://doi.org/10.1590/S1806-66902011000100013>
- Bastos, E. A.; Ramos, H. M. M.; Andrade Júnior, A. S.; Nascimento, F. N.; Cardoso, M. J. Parâmetros fisiológicos e produtividade de grãos verdes do feijão-caupi sob déficit hídrico. *Water Resources and Irrigation Management*, v.1, p.31-37, 2012.
- Bhering, L. L. RBio: A tool for biometric and statistical analysis using the R platform. *Crop Breeding and Applied Biotechnology*, v.17, p.187-190, 2017. <https://doi.org/10.1590/1984-70332017v17n2s29>
- Campeche, L. F. M. S.; Aguiar Netto, A. O.; Sousa, I. F.; Faccioli, G. G.; Silva, V. P. R.; Azevedo, P. V. Lisímetro de pesagem de grande porte. Parte I: Desenvolvimento e calibração. *Revista Brasileira de Engenharia Agrícola e Ambiental*, v.15, p.519-525, 2011. <https://doi.org/10.1590/S1415-43662011000500013>
- Castro Junior, W. L.; Oliveira, R. A.; Silveira, S. F. R.; Andrade Júnior, A. S. Viabilidade econômica de tecnologias de manejo da irrigação na produção do feijão-caupi, na região dos Cocais - MA. *Engenharia Agrícola*, v.35, p.406-418, 2015. <http://dx.doi.org/10.1590/1809-4430-Eng.Agric.v35n3p406-418/2015>
- CONAB - Companhia Nacional de Abastecimento. Acompanhamento da safra brasileira de grãos - safra 2022/2023 - 10º Levantamento. Available on: <https://www.conab.gov.br/info-agro/safras/graos/boletim-da-safra-de-graos/PREVISAO_DE_SAFRA-POR_PRODUTO-JUL-2023.xlsx>. Accessed on: 25/07/2023.
- Digrado, A.; Mitchell, N. G.; Montes, C. M.; Dirvanskyte, P.; Ainsworth, E. A. Assessing diversity in canopy architecture, photosynthesis, and water-use efficiency in a cowpea magic population. *Food Energy Security*, v.9, e236, 2020. <https://doi.org/10.1002/fes3.236>
- Digrado, A.; Gonzalez-Escobar, E.; Owston, N.; Page, R.; Mohammed, S. B.; Umar, M. L.; Boukar, O.; Ainsworth, E. A.; Carmo-Silva, E. Cowpea leaf width correlates with above ground biomass across diverse environments. *Legume Science*, v.4, e144, 2022. <https://doi.org/10.1002/leg3.144>
- Ellsäßer, F.; Röhl, A.; Stiegler, C.; Hendrayanto; Hölscher, D. Introducing QWaterModel, a QGIS plugin for predicting evapotranspiration from land surface temperatures. *Environmental Modelling and Software*, v.130, e104739, 2020. <https://doi.org/10.1016/j.envsoft.2020.104739>
- Ellsäßer, F.; Stiegler, C.; Röhl, A.; June, T.; Hendrayanto; Kohl, A.; Hölscher, D. Predicting evapotranspiration from drone-based thermography - a method comparison in a tropical oil palm plantation. *Biogeosciences*, v.18, p.861-872, 2021. <https://doi.org/10.5194/bg-18-861-2021>
- Ferreira, D. P.; Sousa, D. P.; Nunes, H. G. G. C.; Pinto, J. V. N.; Farias, V. D. S.; Costa, D. L. P.; Moura, V. B.; Teixeira, E.; Sousa, A. M. L.; Pinheiro, H. A.; et al. Cowpea Ecophysiological Responses to Accumulated Water Deficiency during the Reproductive Phase in Northeastern Pará, Brazil. *Horticulturae*, v.7, e116, 2021. <https://doi.org/10.3390/horticulturae7050116>
- Lopes, A. da S.; Andrade Junior, A. S.; Bastos, E.A.; Sousa, C. A. F.; Casari, R. A. C. N.; Moura, M.S.B. Assessment of maize hybrid water status using aerial images from an unmanned aerial vehicle. *Revista Caatinga*, v.37, e11701, 2024. <https://doi.org/10.1590/1983-21252024v37i11701rc>
- Lima, J. R. S.; Antonino, A. C. D.; Hammecker, C.; Lira, C. A. B. O.; Souza, E.S. Water and energy flux measurements in rainfed cowpea cultivated in Northeast Brazil. *Revista Brasileira de Ciências Agrárias*, v.8, p.297-304, 2013.
- Medeiros, M. R.; Cavalcanti, E. P.; Duarte, J. F. M. Classificação climática de Köppen para o estado do Piauí, Brasil. *Revista Equador*, v.9, p.82-99, 2020. <https://doi.org/10.26694/equador.v9i3.9845>
- Melo, F. B.; Souza, H. A.; Bastos, E. A.; Cardoso, M. J. Critical levels and sufficiency ranges for leaf nutrient diagnosis in cowpea grown in the Northeast region of Brazil. *Revista Ciência Agrônômica*, v.51, e20196954, 2020. <https://doi.org/10.5935/1806-6690.20200071>
- Melo, F. B.; Andrade Junior, A. S.; Pessoa, B. L. O. Levantamento, zoneamento e mapeamento pedológico detalhado da área experimental da Embrapa Meio-Norte em Teresina, PI. 2. ed. Teresina: Embrapa Meio-Norte, 2019. 41p.
- Paula, A. C. P.; Silva, C. L.; Rodrigues, L. N.; Scherer-Warren, M. Performance of the SSEBop model in the estimation of the actual evapotranspiration of soybean and bean crops. *Pesquisa Agropecuária Brasileira*, v.54, e00739, 2019. <https://doi.org/10.1590/S1678-3921.pab2019.v54.00739>
- QGIS Development Team. QGIS User Guide, Release 3.22.13: QGIS Project, 2023.
- Senay, G. B.; Mackenzie, F.; Morton, C.; Parrish, G. E. L.; Schauer, M.; Khand, K.; Kagone, S.; Boiko, O.; Huntington, J. Mapping actual evapotranspiration using Landsat for the conterminous United States: Google Earth Engine implementation and assessment of the SSEBop model. *Remote Sensing of Environment*, v.275, e113011, 2022. <https://doi.org/10.1016/j.rse.2022.113011>
- Silva, C. O. F.; Teixeira, A. H. de C.; Manzione, R. L. Agriwater: An R package for spatial modelling of energy balance and actual evapotranspiration using satellite images and agrometeorological data. *Environmental Modelling & Software*, v.120, e104497, 2019. <https://doi.org/10.1016/j.envsoft.2019.104497>
- Silva, J. A.; Barros, J. R. A.; Silva, E. G. F.; Rocha, M. M.; Angelotti, F. Cowpea: Prospecting for heat-tolerant genotypes. *Agronomy*, v.14, e1969, 2024. <https://doi.org/10.3390/agronomy14091969>
- Soil Survey Staff. Keys to Soil Taxonomy. 13.ed. USDA - Natural Resources Conservation Service, 2022. 401p. Available at: <https://www.nrcs.usda.gov/resources/guides-and-instructions/keys-to-soil-taxonomy>. Accessed on: Jan 14, 2025.

- Souza, P. J. O. P.; Farias, V. D. S.; Lima, M. J. A.; Ramos, T. F.; Sousa, A. M. L. Cowpea leaf area, biomass production and productivity under different water regimes in Castanhal, Pará, Brazil. *Revista Caatinga*, v.30, p.748-759, 2017. <https://doi.org/10.1590/1983-21252017v30n323rc>
- Teixeira, A. H. de C. Determining regional actual evapotranspiration of irrigated crops and natural vegetation in the São Francisco river basin (Brazil) using remote sensing and Penman-Monteith equation. *Remote Sensing*, v.2, p.1287-1319, 2010. <https://doi.org/10.3390/rs0251287>
- Timmermans, W. J.; Kustas, W. P.; Andreu, A. Utility of an automated thermal-based approach for monitoring evapotranspiration. *Acta Geophysical*, v.63, p.1571-1608, 2015. <https://doi.org/10.1515/acgeo-2015-0016>
- Vale, B. S.; Roig, H. L.; Neumann, M. R. B.; Fernandes, E. S.; Salles, L. A.; Casari, R. A. C. N.; Olivetti, D.; Malta, E. A. Desempenho dos modelos SEBAL e SSEBop na estimativa da evapotranspiração do trigo no Cerrado. *Revista Brasileira de Meteorologia*, v.7, p.329-345, 2022. <https://doi.org/10.1590/0102-77863730031>
- Xia, T.; Kustas, W. P.; Anderson, M. C.; Alfieri, J. G.; Gao, F.; Mckee, L.; Prueger, J. H.; Geli, H. M. E.; Neale, C. M. U.; Sanchez, L.; Alsina, M. M.; Wang, Z. Mapping evapotranspiration with high-resolution aircraft imagery over vineyards using one- and two-source modeling schemes. *Hydrology and Earth System Sciences*, v.20, p.1523-1545, 2016. <https://doi.org/10.5194/hess-20-1523-2016>